Received: 3 June 2020 | Revised: 5 October 2020 | Accepted: 6 October 2020
DOI: 10.1002/joc.6871

RESEARCH ARTICLE

International Journal of Climatology RMetS

Interdecadal summer warming of the Tibetan Plateau potentially regulated by a sea surface temperature anomaly in the Labrador Sea

Kailun Gao[1,2] | Anmin Duan[1,2,3] | Deliang Chen[4]

[1]State Key Laboratory of Numerical Modeling for Atmospheric Sciences and Geophysical Fluid Dynamics, Institute of Atmospheric Physics, Chinese Academy of Sciences, Beijing, China
[2]College of Earth and Planetary Sciences, University of Chinese Academy of Sciences, Beijing, China
[3]Key Laboratory of Meteorological Disaster and Collaborative Innovation Center on Forecast and Evaluation of Meteorological Disasters, Nanjing University of Information Science & Technology, Nanjing, China
[4]Regional Climate Group, Department of Earth Sciences, University of Gothenburg, Gothenburg, Sweden

Correspondence
Anmin Duan, State Key Laboratory of Numerical Modeling for Atmospheric Sciences and Geophysical Fluid Dynamics, Institute of Atmospheric Physics, Chinese Academy of Sciences, Beijing 100029, China.
Email: amduan@lasg.iap.ac.cn

Funding information
Strategic Priority Research Program of the Chinese Academy of Sciences XDA19070404 XDA20060401; National Natural Science Foundation of China, Grant/Award Numbers: 41725018, 91637312

Abstract
Downward clear-sky longwave radiation, which is related to atmospheric water vapour content, has been suggested as an important factor causing an interdecadal increase in boreal summer surface temperature over the Tibetan Plateau (TP). We reveal the relationship between the 2 m air temperature (t2m) and water vapour over the TP in boreal summer, as well as the mechanism modulating the change in atmospheric water vapour. In recent decades, spatiotemporal variations between water vapour and t2m in boreal summer over the TP have shown synchronicity at the decadal scale. Moreover, Rossby wave trains which originate over the Northwest Atlantic and trigger an anomalous anticyclone between the northeastern TP and Baikal Lake are suggested to play a crucial role in decadal warming over the TP. First, the anomalous anticyclone, with an equivalent barotropic structure, can directly heat near-surface air across the northeastern TP. Second, it promotes net water vapour input into the northeastern TP, leading to an increase of the total water vapour content over the entire TP, ultimately contributing to warming. Finally, a linear baroclinic model experiment further indicates that the Rossby wave trains are mainly associated with interdecadal increases in sea surface temperature (SST) in the Labrador Sea, with the SST in Baffin Bay playing a secondary role.

KEYWORDS
2 m air temperature, decadal variation, Labrador Sea, Tibetan plateau, water vapour

1 | INTRODUCTION

The Tibetan Plateau (TP), called the Earth's 'Third Pole' because of its unique topography (Qiu, 2008), has a critical influence on regional and global climate via thermal and dynamic forcing (Zhou *et al.*, 2009; Duan *et al.*, 2012; Wu *et al.*, 2012). The warming trend over the TP in the last half century has been stronger than that in other regions at the same latitude during the same period (Liu and Chen, 2000). Therefore, as both an important and sensitive region, climate change and its impacts on the TP have attracted increasing attention.

Wang *et al.* (2008) found a warming trend in annual mean surface temperature over the TP of 0.36°C per decade during 1961–2007, which is double the previous estimate based on 1955–1996 data (Liu and Chen, 2000). Furthermore, in contrast to the recent global warming hiatus, an accelerated warming trend has been observed over the TP since the end of the 1990s (Duan and Xiao, 2015; You *et al.*, 2016).

An increase in 2 m air temperature in summer has played a primary role in the rapid increase in annual mean air temperature since the mid-1980s across the northern TP (Guo and Wang, 2011). Application of the dynamic adjustment method by Ma *et al.* (2017) showed that radiatively forced temperature over the TP played a dominant role in accelerated warming, but other reasons have also been proposed; these include changes in the surface albedo feedback (Ghatak *et al.*, 2014; Pepin *et al.*, 2015; You *et al.*, 2016), the enhanced greenhouse effect (Liu and Chen, 2000; Chen *et al.*, 2003), changes in water vapour and cloud amounts (Duan and Wu, 2006; Rangwala *et al.*, 2013) and changes in near-surface radiation fluxes (Yan *et al.*, 2016). Multidecadal or millennial variability of surface temperature over the TP seems to be closely related to the Atlantic multidecadal oscillation or Atlantic multidecadal variability, according to proxy records (Wang *et al.*, 2013a; 2013b; Shi *et al.*, 2017; 2019). However, the mechanism driving this decadal temperature pattern over the TP is still an open question.

The TP is known as the 'Asian water tower' because of its important role in the hydrological cycle (Xu *et al.*, 2008; Immerzeel *et al.*, 2010). Since atmospheric water vapour capacity increases with temperature (according to the Clausius–Clapeyron equation: Trenberth, 2011), changes in water vapour and precipitation over the TP associated with accelerated warming are critical for the downstream regions. Previous studies have shown that precipitation and water vapour over the TP are greatest in summer (You *et al.*, 2012; Zhang *et al.*, 2013; You *et al.*, 2015), accounting for ~60–70% of annual precipitation (Liu and Yin, 2001; Sui *et al.*, 2013). The precipitable water in the atmosphere of the TP has increased significantly since the 1990s (Zhang *et al.*, 2013), but the spatial pattern of changes in precipitation is complicated and heterogeneous (Kuang and Jiao, 2016). Possible causes of such complex patterns have been discussed in previous studies. For example, Gao *et al.* (2014) found that the TP has become wetter, albeit with large spatial variations, by decomposing the changes in precipitation minus evaporation into three major components—dynamic, thermodynamic and transient eddy components—with the results showing that the dynamic component had contributed positively to the changing patterns of precipitation and evaporation during the wet season. The Asian summer monsoon, which is influenced by the TP thermal state and glacier extent (Wu *et al.*, 2012; Yao *et al.*, 2012), is also a key carrier for the transport of water vapour over the TP in summer (Fu *et al.*, 2006; Xu *et al.*, 2014). Most recent studies (Gao *et al.*, 2019; Wu *et al.*, 2020) have found that downward clear-sky longwave radiation, which is related to atmospheric water vapour content, can be the dominant factor causing warming over the TP; this effect is stronger during the boreal summer than other seasons. In this paper, we will further explore the drivers of the water vapour changes responsible for summer warming over the TP.

2 | DATA, MODEL AND METHODS

We used the monthly Japanese 55-year reanalysis (JRA-55) dataset for the period 1980–2017 along with model data (TL319L60) developed by the Japan Meteorological Agency (Ebita *et al.*, 2011; Kobayashi *et al.*, 2015). The reanalysis dataset includes surface temperature (T_s), 2 m air temperature (t2m), u and v components of wind, geopotential height, specific humidity and precipitable water. Zhao and Zhou (2019) have demonstrated that JRA-55 performs best at capturing interannual water vapour variability compared with satellite and other reanalysis datasets. To quantify changes in sea surface temperature (SST), we used the fifth version of the NOAA Extended Reconstructed Sea Surface Temperature (ERSST) (Huang *et al.*, 2017), with a horizontal resolution of $2^\circ \times 2^\circ$. The region of the TP focused on in this work is displayed in Figure 1, which outlines the area of interest with an altitude higher than 2000 m.

The linear baroclinic model (LBM), developed by the Center for Climate System Research, University of Tokyo, is a linearized atmospheric model with a simplified dynamic framework (Watanabe *et al.*, 1999; Watanabe and Kimoto, 2000). The LBM can help us understand the complicated atmospheric feedbacks by removing certain nonlinear processes. Thus, the results were the directly linear response to the forcings. Here, the LBM was used to simulate the atmospheric response to a positive Northwest Atlantic SST anomaly. When using the model, we set only the SST forcing in location and intensity; the others were kept to default settings. The reference state is the T42L20 model from the boreal summer (June–July–August) climatology for 1979–2014 in the NCEP/NCAR reanalysis data.

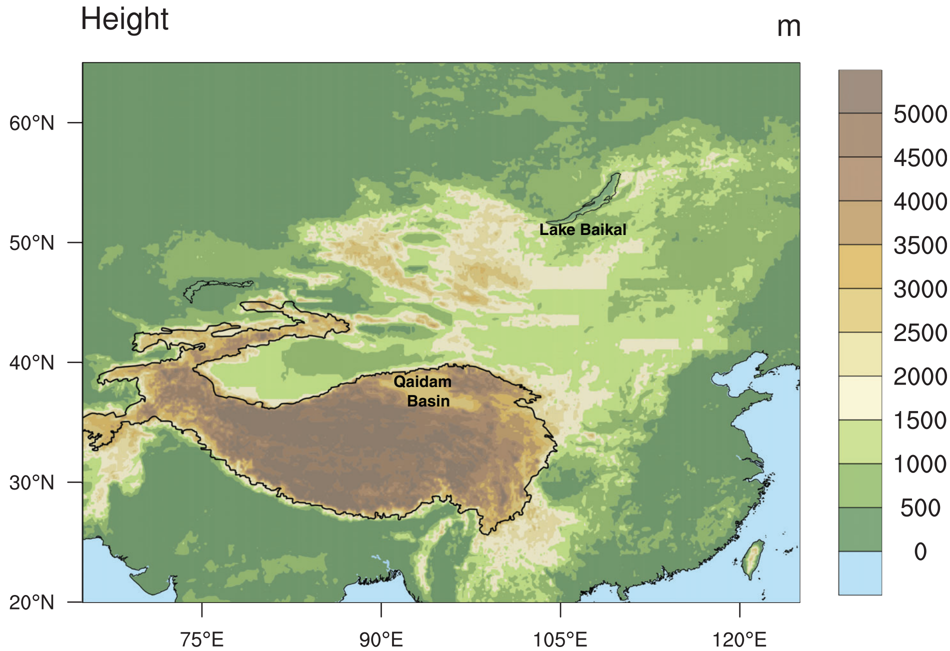

FIGURE 1 The black curve outlines the area of the Tibetan Plateau (TP, 70–105°E, 25–40°N) studied in this paper with an averaged altitude higher than 2000 m

To examine changes in water vapour over TP, the vertically integrated water vapour flux Q and divergence of water vapour flux Q_{div} were calculated as follows:

$$Q=\frac{1}{g}\int_{p_0}^{p_1} q\vec{V}\mathrm{d}p,\ Q_{\mathrm{div}}=\frac{1}{g}\int_{p_0}^{p_1}\nabla\left(q\vec{V}\right)\mathrm{d}p.$$

Here, we chose p_0=600 hPa and p_1=300 hPa, because the surface pressure is around 600 hPa over the TP and the water vapour content is negligible above 300 hPa (Zhang *et al.*, 2013).

To obtain the decadal signals of selected variables, a 9-year Lanczos low-pass filter (Duchon, 1979) was used. In addition, the 3D wave activity flux derived by Takaya and Nakamura (2001) (hereafter the T–N wave activity flux) was used to diagnose the propagation of Rossby eddies. Standard empirical orthogonal function (EOF) analysis (Weare and Newell, 1977; Weare and Nasstrom, 1982) was used to identify the main spatiotemporal patterns of t2m and atmospheric water vapour over the TP in the study, and the Student's *t* test (two-tailed) was used to assess statistical significance.

3 | RESULTS

3.1 | Coincident spatiotemporal variability in summer precipitable water and t2m over the TP

The Lanczos 9-point filter is used to assess the temporal variability in precipitable water and t2m by capturing the decadal signals. Analysis of the JRA-55 dataset reveals that interdecadal changes in t2m and precipitable water during boreal summer show the same characteristic: specifically, the shift from a negative anomaly to a positive anomaly between 1997 and 1998 significant at the 95% confidence level (Figure 2a,b). The time series are thus divided into two periods: 1980–1997 and 1998–2017. The correlation between t2m and precipitable water reached 0.96, which exceeds the 99% confidence level. The difference in spatial distribution of t2m over the TP between 1980–1997 and 1998–2017 (hereafter this means 1998–2017 minus 1980–1997) indicates overall warming, except in the Himalayas where there is cooling of less than -1 K, and areas with warming exceeding 1.5 K are located in the northern TP and Qaidam Basin (Figure 2c). Wang *et al.* (2014) also found that the warming rate in the Qaidam Basin, in the northeastern TP, was much higher than that in other regions over the TP. The spatial distribution of precipitable water showed a uniform increase between 1980–1997 and 1998–2017; those regions with the greatest increase also coincided with the regions showing the greatest increase in t2m (Figure 2d). In some regions, precipitable water increased by more than 2 $\mathrm{kg{\cdot}m^{-2}}$ between the two periods.

Furthermore, EOF analysis was used to assess whether the above temporal and spatial variations represent the dominant patterns. EOF analysis for t2m (Figure 3a,b) indicated that the first leading model (EOF1) accounted for 48.8% of the total variance. As EOF1 has the largest variance, its corresponding pattern was the most widespread, hence the areas with the most significant changes appeared in the northern and northeastern TP (Figure 3a), and the associated interdecadal signal from negative to positive, extracted with the Lanczos 9-point filter, can also be seen in the first

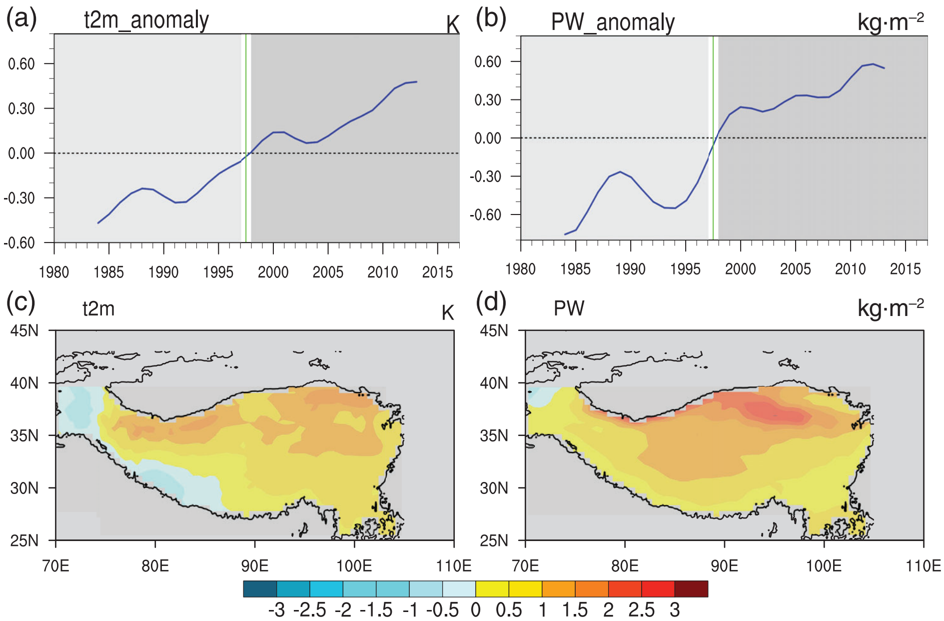

FIGURE 2 Summer (June–July–August) interdecadal variations in (a) 2 m air temperature (t2m) and (b) precipitable water (PW) over the TP, processed with a Lanczos 9-point filter. (c) The spatial distribution of the difference in summer t2m between 1998 and 2017 and 1980–1997. (d) As in (c), but for summer PW

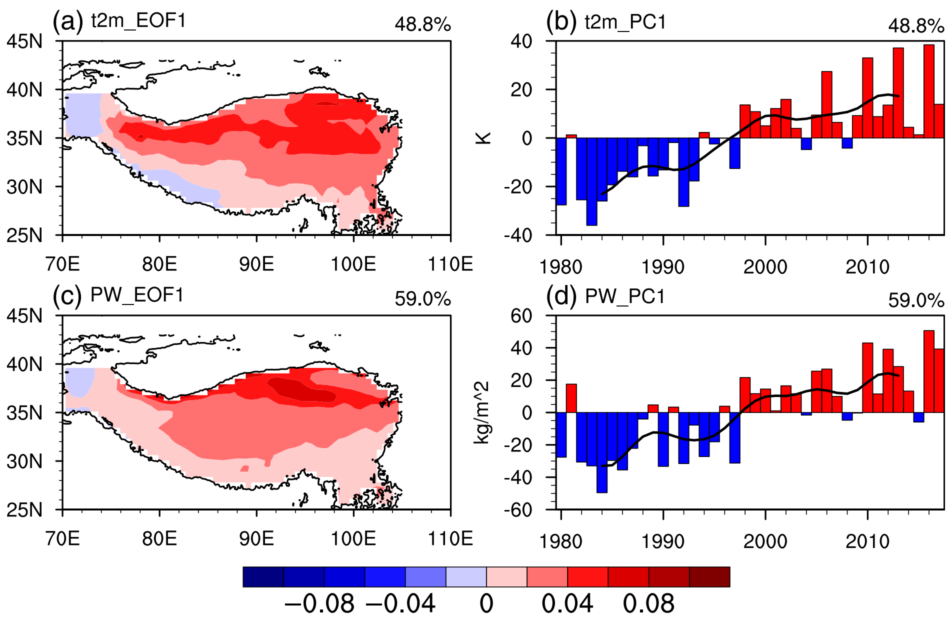

FIGURE 3 (a)–(b) The empirical orthogonal function (EOF) analysis for summer t2m over the TP: (a) shows the first model (EOF1) and (b) is the first principal component time series (PC1) showing interdecadal variations (black solid curve; unit: K). (c) and (d) are the same as (a) and (b), respectively, but for PW (unit: kg · m^{-2})

principal component (PC1) time series (the black solid curve in Figure 3b). Meanwhile, water vapour showed a uniform pattern within its respective EOF1, whose explained variance was up to 58.8% (Figure 3c) with the largest variation region found in the Qaidam Basin. The same interdecadal variation in PC1 time series as t2m is also displayed (Figure 3d). A comparison of these two EOF1 patterns shows that the regions with the greatest magnitudes or time series with interdecadal increase in 1997/98 were consistent between both t2m and water vapour. The EOF1s of t2m and water vapour over the TP reveal that the interdecadal spatiotemporal variability in boreal summer was their common and dominant feature in recent decades.

The vertically integrated water vapour flux (Q) is often used to analyse moisture transport pathways, represented as net water vapour inputs to the TP from the eastern and southern boundaries and outputs from the northern boundary (Figure 4a). Moreover, water vapour flux divergence (Q_{div}) is a useful index with which to examine the strength of a water vapour source/sink (Howarth, 1986). Strong moisture convergence is observed over the TP along its southeastern edge, northwestern edge and over Qinghai Lake where it exceeds -2 kg·m^{-2} · s^{-1}. In comparison, strong divergence along its southwestern edge (along the Himalayas) reaches maximum values of 2 kg·m^{-2} · s^{-1} (Figure 4a). These regions closely match those with conspicuous warming

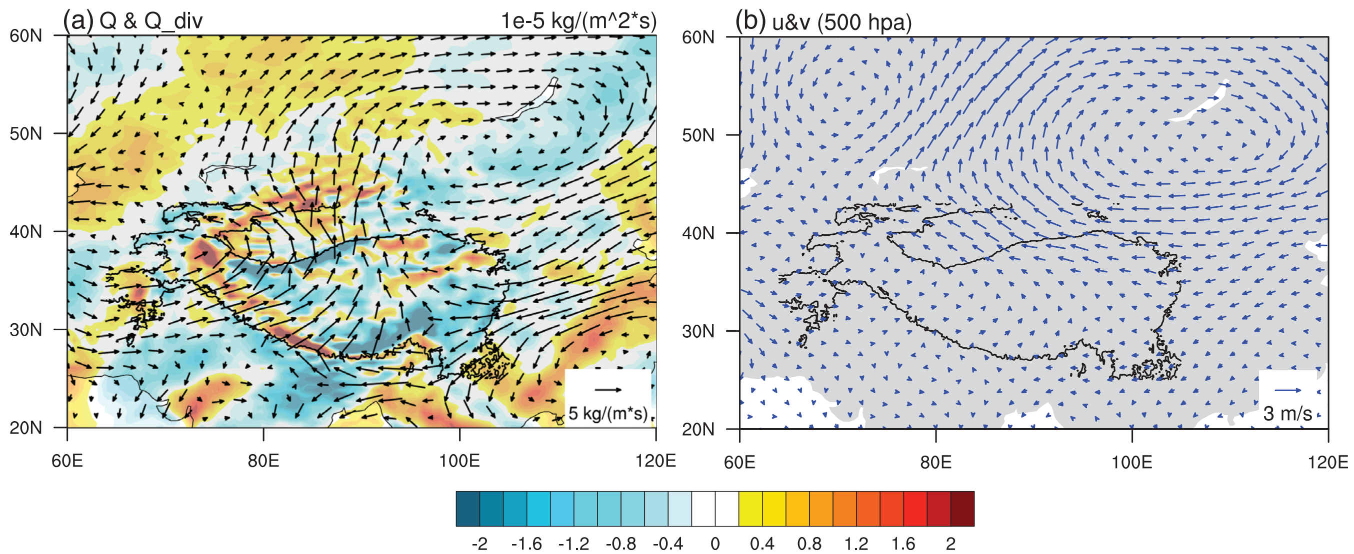

FIGURE 4 (a) Difference (1998–2017 minus 1980–1997) in vertically integrated water vapour flux (Q) (shaded; unit: 10^{-5} kg·m^{-2}·s^{-1}) and water vapour flux divergence (Q_{div}) from 600 to 300 hPa in summer (vectors; unit: kg · m^{-1} · s^{-1}). (b) Difference in 500 hPa u–v composite between 1998–2017 and 1980–1997

or cooling across the TP (Figure 2c), further confirming that warming over the TP is dominated by the increase of water vapour in boreal summer, which has also been diagnosed by the surface energy budget equilibrium equation (Gao *et al.*, 2019). Therefore, we now explore what processes have influenced the increase in water vapour in recent decades.

3.2 | The origin of the anomalous anticyclone between the northeastern TP and Lake Baikal

Atmospheric circulation is one of the main controls over water vapour transport. The change in the 500 hPa wind field between 1980–1997 and 1998–2017 (Figure 4b) reveals the development of an anomalous anticyclone between the northeastern TP and Lake Baikal, where it has played a key role in strengthening net moisture input from the eastern boundary (Figure 4a); this will lead to an increase in total water vapour content across the TP.

To reveal the origin of the anomalous anticyclone, differences in the 200 hPa geopotential height eddy (which refers to the departure of geopotential height from the zonal mean) and T–N wave activity fluxes between 1980–1997 and 1998–2017 were examined (Figure 5a). Rossby wave trains propagate from the Labrador Sea to the northeastern TP, and the T–N wave activity flux showed that wave energy propagates along this same pathway. Positive 200 hPa height anomalies were located in the Northwest Atlantic, Central Europe and southwest Lake Baikal, while negative anomalies were located in

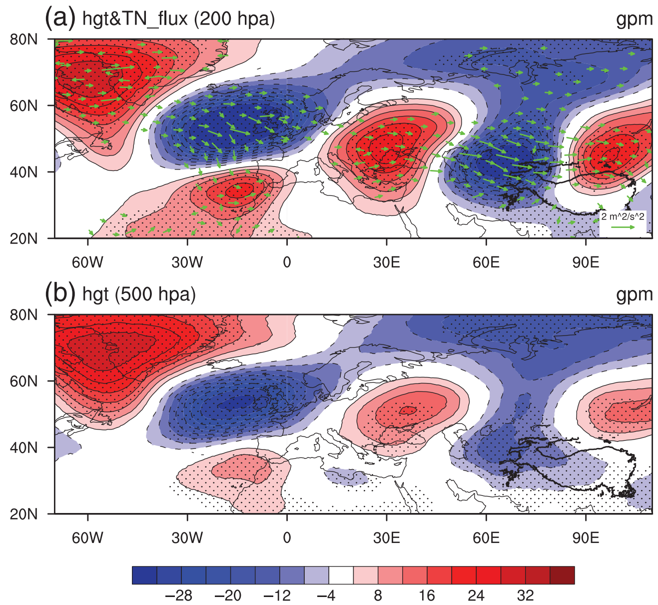

FIGURE 5 (a) Difference (1998–2017 minus 1980–1997) in zonal perturbation at 200 hPa (shaded; unit: gpm) and T–N wave activity flux (vectors; unit: m^2 · s^{-2}). (b) Difference in zonal perturbation at 500 hPa geopotential height (shaded; unit: gpm). The dotted area in both panels indicates significance at the 95% confidence level

the Central Eastern Atlantic and Western Asia; peak magnitudes of these anomalies exceeded 30 gpm and were significant at the 95% confidence level. A similar pattern of anomalies, also significant at the 95% confidence level, was found at 500 hPa (Figure 5b) in regions generally consistent with those at 200 hPa, reflecting the equivalent barotropic structure of the geopotential

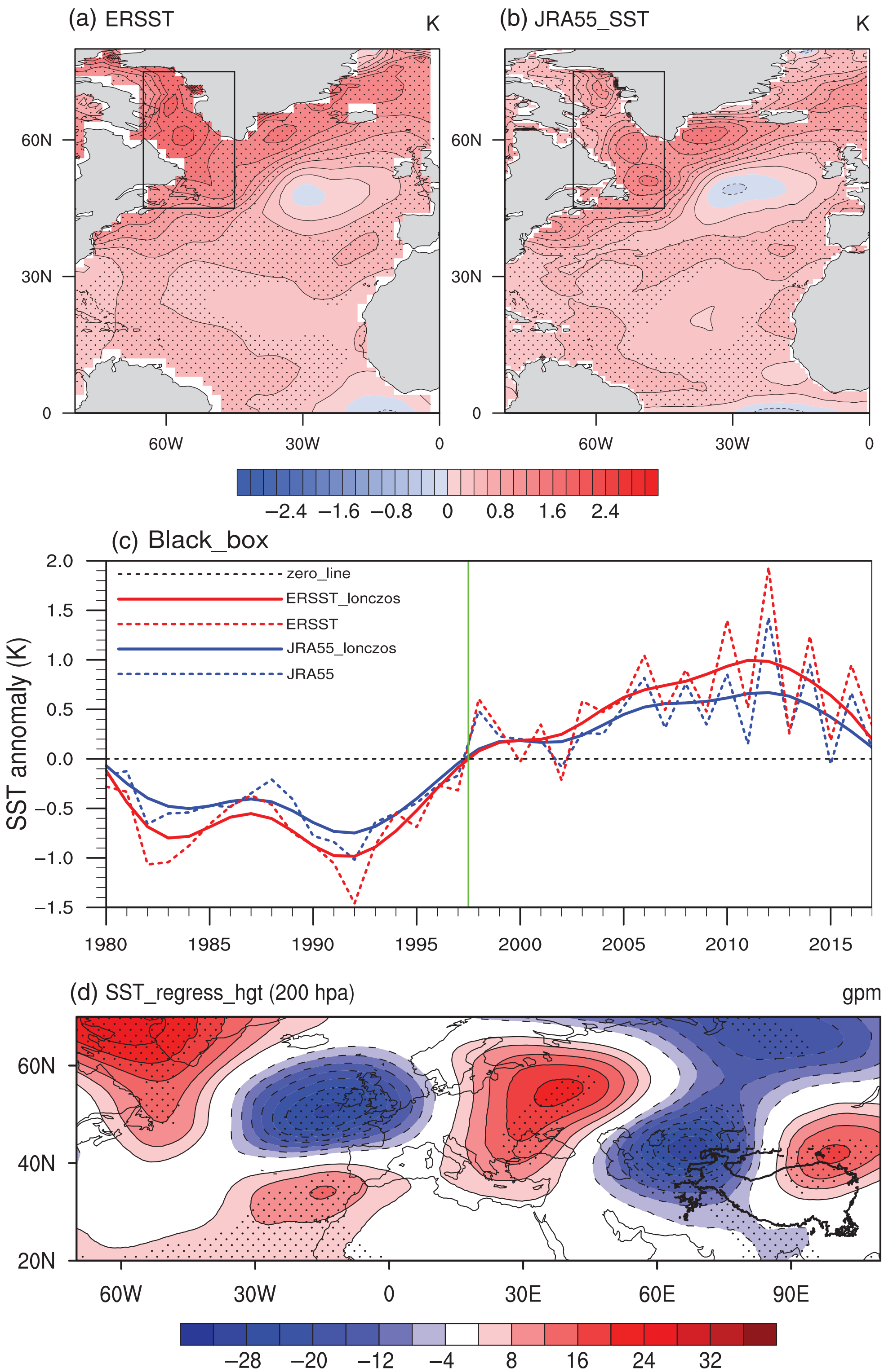

FIGURE 6 Difference in summer sea surface temperature (SST) between 1998–2017 and 1980–1997 in (a) the ERSST dataset and (b) the JRA-55 dataset, with dotted areas indicating significance at the 95% confidence level. The study region is shown by the black box. (c) Temporal variations in SST anomaly in the regions shown by the black box; solid curves show interdecadal changes. (d) Interdecadal variations of SST in the ERSST dataset regressed against the 200 hPa geopotential height (unit: gpm), with dotted areas indicating significance at the 95% confidence level

height. This indicates that the anomalous anticyclone originated from the Labrador Sea or Baffin Bay.

The difference in North Atlantic summer SST between 1980–1997 and 1998–2017 (Figure 6a,b) shows that the areas with the strongest increase in SST (exceeding 2K) are mainly in the Northwest Atlantic (as marked by the black box in Figure 6), including the Labrador Sea, Davis Strait and southeast Baffin Bay. Temporal changes in the SST anomaly in the area of the black box (Figure 6c) indicate that a similar interdecadal warming also occurred in the Northwest Atlantic; the turning point from a negative anomaly to a positive anomaly was also between 1997 and 1998, coincident with the interdecadal shift in t2m over the TP in summer. Regressing the interdecadal SST anomaly in the black box against 200 hPa geopotential height yields a remarkably similar pattern to that in Figure 5a at the 95% confidence level (Figure 6d), which indicates that the origin of the anomalous anticyclone over the northeastern TP was interdecadal warming of the Northwest Atlantic SST. However, which sea sector in the Northwest Atlantic plays a key role still remains to be verified.

3.3 | LBM experiments

The LBM, which is often used to present the main atmospheric dynamic process, was applied to further verify the process driving the influence of interdecadal change in the Northwest Atlantic SST on summer t2m over the TP. According to the reanalysis data, the maximum increase areas in SST were located mainly in the Labrador Sea and southeast Baffin Bay. Therefore, two experiments were designed, based on the two centres' value and location of SST in the black box (Figure 6a,b). Both experiments added an elliptical area of additional heating, firstly in the Labrador Sea, centred at 65°N, 58°W (Figure 7b), and secondly in southeast Baffin Bay, centred at 71°N, 60°W (Figure 8b). The integral of the vertical heating rate was 2K per day in the first forcing (Figure 7a), with a similar forcing in the second experiment (Figure 8a). The responses had not equilibrated

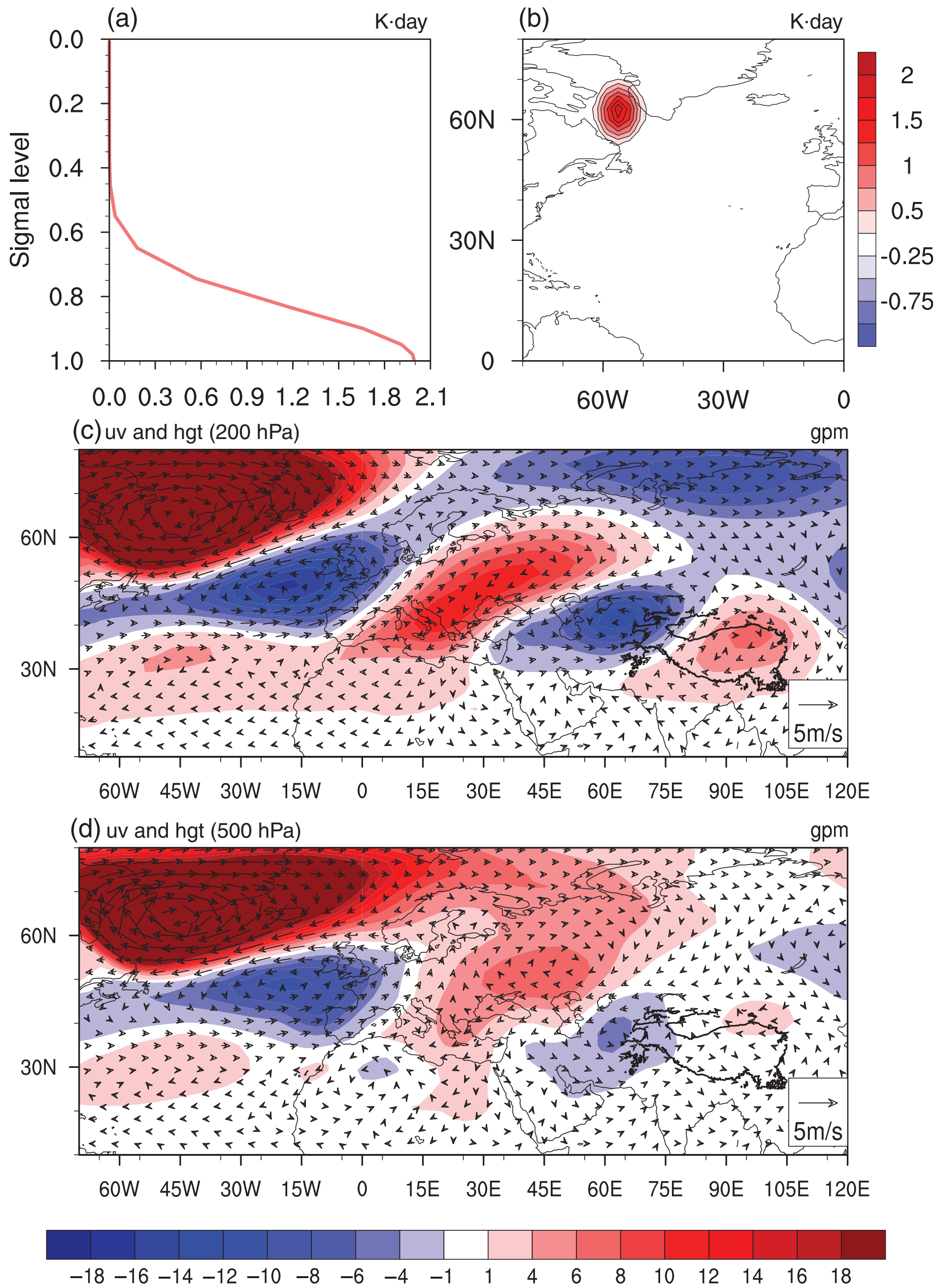

FIGURE 7 Forcing of the linear baroclinic model (LBM) experiment in the Labrador Sea: (a) the diabatic heating profile of the forcing centre (unit: K·day^{-1}), and (b) the SST forcing pattern (unit: K·day^{-1}). (c) the response at 200 hPa, including the geopotential height (shaded; unit: Gpm) and u–v velocity composite (vectors; unit: m s^{-1}). (d) As in (c), but at 500 hPa

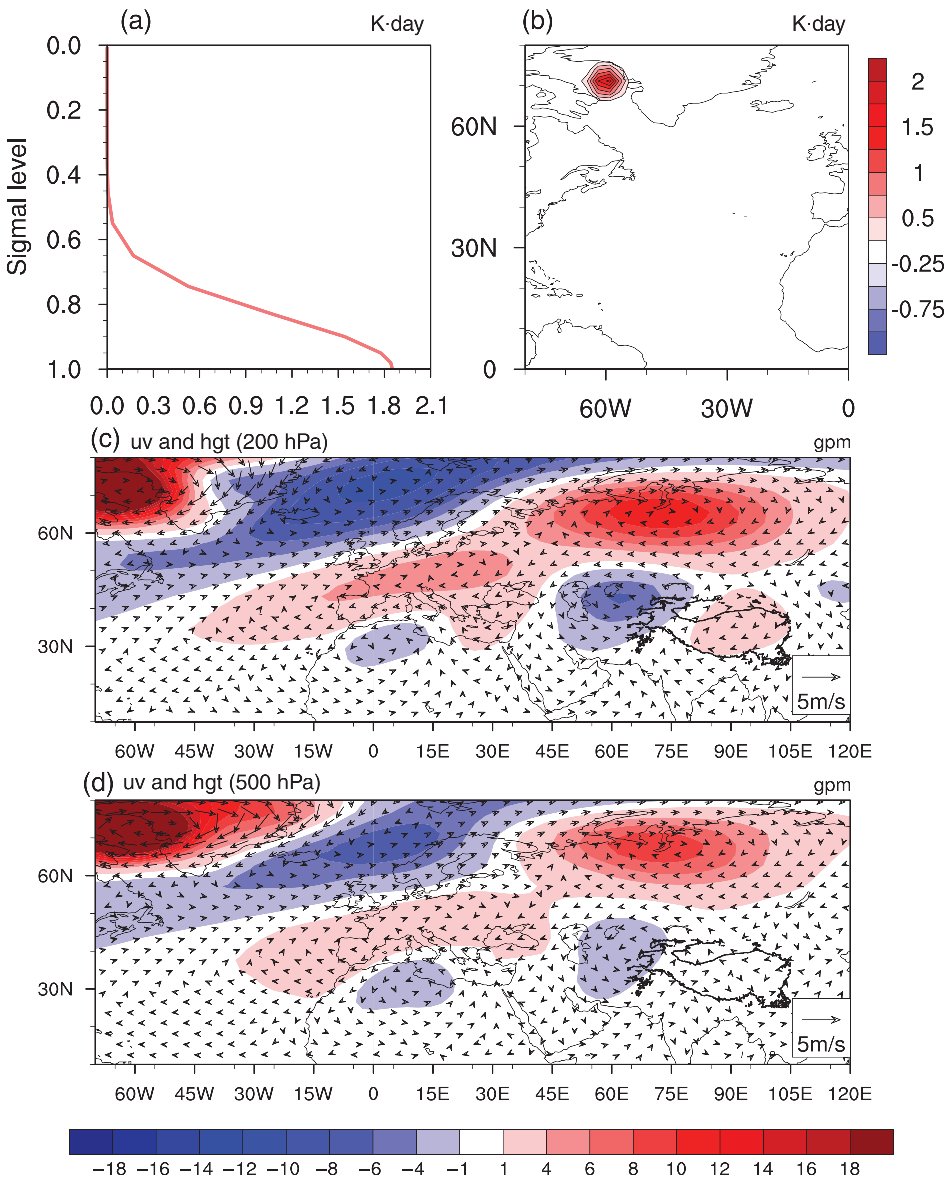

FIGURE 8 As for Figure 7, but for the forcing in Baffin Bay

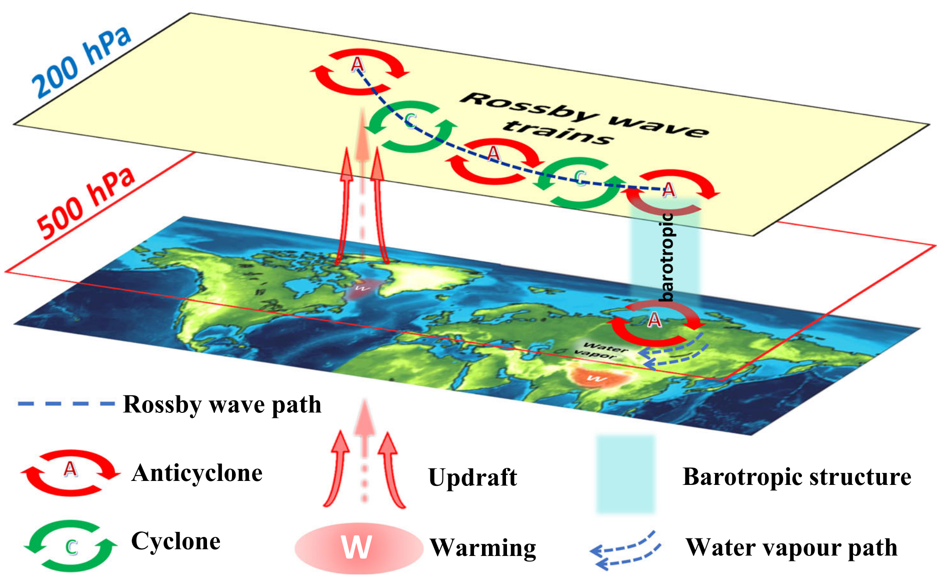

FIGURE 9 Schematic diagram showing how the interdecadal positive SST anomaly in the Labrador Sea modulates interdecadal summer warming over the TP

until day 20 in the simulations because the forcings were located at high latitudes (Jin and Hoskins, 1995). Therefore, we used a 30-day integration and analysed the mean response from days 20 to 30.

The results reveal similar Rossby wave trains at 200 hPa when the heat source was located in the Labrador Sea (Figure 7c), with an anomalous anticyclone over the northeastern TP. Meanwhile, a relatively weak anomalous anticyclone over the northeastern TP at 500 hPa (Figure 7d) demonstrated the existence of an equivalent barotropic structure. In contrast, when the heat source was located in southeast Baffin Bay, the signal was similar but much weaker at 200 hPa (Figure 8c), and the anomalous anticyclone was even not visible over the northeastern TP at 500 hPa (Figure 8d). Therefore, the Rossby wave trains are stimulated by a positive SST anomaly in the Labrador Sea, with other regions in the Northwest Atlantic playing a supporting role.

4 | CONCLUSION AND DISCUSSION

Variations in t2m across the TP were found to be significantly correlated with water vapour at the decadal scale, and differences between 1980–1997 and 1998–2017 in both t2m and water vapour share similar spatial characteristics. Moreover, EOF analysis indicated that this consistency reflects their similar EOF1s, not only in terms of interdecadal changes, but also their spatial patterns.

Further analysis indicated a Rossby wave train propagating from the Northwest Atlantic to the northeastern TP. T–N wave activity flux diagnosis confirmed that the waves originate from the Labrador Sea or Baffin Bay and trigger an anomalous anticyclone over the northeastern TP and Baikal Lake. This anomalous anticyclone, with an equivalent barotropic structure, not only directly heats the near-surface air across the northeastern TP but also promotes net water vapour transport to the TP, causing atmospheric warming through the increase of the total water vapour content, which further explained the mechanism that led to increased downward clear-sky longwave radiation in boreal summer over the entire TP (Gao *et al.*, 2019). The LBM experiment further confirmed that the interdecadal increase in Labrador SST played the dominant role in stimulating the Rossby wave trains, rather than Baffin Bay SST. A schematic diagram of this complete process is provided in Figure 9.

Numerous studies have found that Atlantic multidecadal variability (AMV) related to the Atlantic meridional overturning circulation (AMOC) has played an important role in some important climate impacts (Zhang *et al.*, 2019). Kim *et al.* (2020) used coupled ensemble experiments designed to isolate the climate response to buoyancy forcing associated with the North Atlantic Oscillation in the Labrador Sea, proving that ocean dynamical changes are the essential drivers of AMV but that atmospheric teleconnections influence the full AMV pattern by transmitting the Labrador SST signal into the rest of the basin. However, whether the Labrador Sea Water formation is really related to the AMOC is still under debate (Pickart and Spall, 2007; Zhang, 2010; Kwon and Frankignoul, 2014; Li *et al.*, 2019). Future work should further explore this possible relationship, as this may help us to understand how the AMOC influences climate change in remote regions by regulating SST variations in the Labrador Sea.

Certainly, a number of other possible factors affecting the TP warming in boreal summer have also been discussed in past studies, such as surface albedo feedback, changes in cloud amount and land surface greening in the TP. Not only has snowfall decreased with TP warming in summer (Deng *et al.*, 2017), but the snow cover has retreated, which has further enhanced the warming by surface albedo positive feedback (You *et al.*, 2016). The cloud amount, with different changes in daytime and at nighttime, also contributed to warming over the TP (Duan and Wu, 2006). The declining cloud cover may have been caused by the weakening of both the South Asian summer monsoon and local-scale atmospheric upward motion in boreal summer (Ji *et al.*, 2020). Other studies (Chapin *et al.*, 2005; Pearson *et al.*, 2013) found that increased vegetation productivity by reducing albedo could cause a positive feedback on surface warming, although Shen *et al.* (2015) suggested that increased vegetation activity may have attenuated daytime warming by enhancing evapotranspiration over the TP. Therefore, exploring the mechanisms and relative importance of these factors needs to be continued in the future.

ACKNOWLEDGEMENTS

This work was supported by the Strategic Priority Research Program of the Chinese Academy of Sciences (grant numbers XDA19070404 and XDA20060401) and the National Natural Science Foundation of China (grant numbers 41725018 and 91637312). All data used in this study can be publicly downloaded online. The Japanese 55-year reanalysis (JRA-55) dataset is from ftp://ds.data.jma.go.jp. The fifth version of the NOAA Extended Reconstructed Sea Surface Temperature (ERSST) is from https://catalog.data.gov/dataset/extended-reconstructed-sea-surface-temperature-ersst.

ORCID

Kailun Gao https://orcid.org/0000-0001-6081-7141
Deliang Chen https://orcid.org/0000-0003-0288-5618

REFERENCES

Chapin, F.S.I.I.I., Sturm, M., Serreze, M.C., McFadden, J.P., Key, J.R., Lloyd, A.H., McGuire, A.D., Rupp, T.S., Lynch, A.H., Schimel, J.P., Beringer, J., Chapman, W.L., Epstein, H.E., Euskirchen, E.S., Hinzman, L.D., Jia, G., Ping, C.-L., Tape, K.D., Thompson, C.D.C., Walker, D.A. & Welker, J.M. (2005) Role of land-surface changes in arctic summer warming. *Science*, 310, 657–660.

Chen, B., Chao, W. and Liu, X. (2003) Enhanced climatic warming in the Tibetan Plateau due to doubling CO2: a model study. *Climate Dynamics*, 20, 401–413.

Deng, H., Pepin, N.C. and Chen, Y. (2017) Changes of snowfall under warming in the Tibetan Plateau. *Journal of Geophysical Research: Atmosphere*, 122, 7323–7341.

Duan, A. and Wu, G. (2006) Change of cloud amount and the climate warming on the Tibetan Plateau. *Geophysical Research Letters*, 33, L22704.

Duan, A., Wu, G., Liu, Y., Ma, Y. and Zhao, P. (2012) Weather and climate effects of the Tibetan Plateau. *Advances in Atmospheric Sciences*, 29, 978–992.

Duan, A. and Xiao, Z. (2015) Does the climate warming hiatus exist over the Tibetan Plateau? *Scientific Reports*, 5, 13711.

Duchon, C. (1979) Lanczos filtering in one and two dimensions. *Journal of Applied Meteorology*, 18, 1016–1022.

Ebita, A., Kobayashi, S., Ota, Y., Moriya, M., Kumabe, R., Onogi, K., Harada, Y., Yasui, S., Miyaoka, K., Takahashi, K., Kamahori, H., Kobayashi, C., Endo, H., Soma, M., Oikawa, Y., Ishimizu, T. (2011) The Japanese 55-year reanalysis “JRA-55”: an interim report. *SOLA*, 7, 149–152.

Fu, R., Hu, Y., Wright, J.S., Jiang J.H., Dickinson, R.E., Chen, M., Filipiak, M., Read, W.G., Waters, J.W. & Wu, D.L. (2006) Short circuit of water vapor and polluted air to the global stratosphere by convective transport over the Tibetan Plateau. *Proceedings of the National Academy of Sciences of the United States of America*, 103, 5664–5669.

Gao, K., Duan, A., Chen, D. and Wu, G. (2019) Surface energy budget diagnosis reveals possible mechanism for the different warming rate among Earth's three poles in recent decades. *Science Bulletin*, 64, 1140–1143.

Gao, Y., Cuo, L. and Zhang, Y. (2014) Changes in moisture flux over the Tibetan Plateau during 1979–2011 and possible mechanisms. *Journal of Climate*, 27, 1876–1893.

Ghatak, D., Sinsky, E. and Miller, J. (2014) Role of snow-albedo feedback in higher elevation warming over the Himalayas, Tibetan Plateau and Central Asia. *Environmental Research Letters*, 9, 114008.

Guo, D. and Wang, H. (2011) The significant climate warming in the northern Tibetan Plateau and its possible causes. *International Journal of Climatology*, 32, 1775–1781.

Howarth, D.A. (1986) An analysis of the water vapor flux divergence field over the southern hemisphere. *Annals of the Association of American Geographers*, 76, 190–207.

Huang, B., Thorne, P.W., Banzon, V.F., Boyer, T., Chepurin, G., Lawrimore, J.H., Menne, M.J., Smith, T.M., Vose, R.S. and Zhang, H.-M. (2017) Extended reconstructed sea surface temperature version 5 (ERSSTv5), upgrades, validations, and intercomparisons. *Journal of Climate*, 30, 8179–8205.

Immerzeel, W.W., van Beek, L.P.H. and Bierkens, M.F.P. (2010) Climate change will affect the Asian water towers. *Science*, 328, 1382–1385.

Ji, P., Yuan, X. and Li, D. (2020) Atmospheric radiative processes accelerate ground surface warming over the southeastern Tibetan Plateau during 1998-2013. *Journal of Climate*, 33, 1881–1895.

Jin, F.F. and Hoskins, B.J. (1995) The direct response to tropical heating in the baroclinic atmosphere. *Journal of the Atmospheric Sciences*, 52, 307–319.

Kim, W.M., Yeager, S. and Danabasoglu, G. (2020) Atlantic multidecadal variability and associated climate impacts initiated by ocean Thermohaline dynamics. *Journal of Climate*, 33, 1317–1334.

Kobayashi, S., Ota, Y., Harada, Y., Ebita, A., Moriya, M., Onoda, H., Onogi, K., Kamahori, H., Kobayashi, C., Endo, H., Miyaoka, K. & Takahashi, K. (2015) The JRA-55 reanalysis: general specifications and basic characteristics. *Journal of the Meteorological Society of Japan*, 93, 5–48.

Kuang, X. and Jiao, J. (2016) Review on climate change on the Tibetan Plateau during the last half century. *Journal of Geophysical Research: Atmosphere*, 121, 3979–4007.

Kwon, Y.-O. and Frankignoul, C. (2014) Mechanisms of multidecadal Atlantic meridional overturning circulation variability diagnosed in depth versus density space. *Journal of Climate*, 27, 9359–9376.

Li, F., Lozier, M.S., Danabasoglu, G., Holliday, N.P., Kwon, Y.-O., Romanou, A., Yeager, S.G. and Zhang, R. (2019) Local and downstream relationships between Labrador Sea water volume and North Atlantic Meridional overturning circulation variability. *Journal of Climate*, 32, 3883–3898.

Liu, X. and Chen, D. (2000) Climatic warming in the Tibetan Plateau during recent decades. *International Journal of Climatology*, 20, 1729–1742.

Liu, X. and Yin, Z. (2001) Spatial and temporal variation of summer precipitation over the eastern Tibetan Plateau and the North Atlantic oscillation. *Journal of Climate*, 14, 2896–2909.

Ma, J., Guan, X., Guo, R., Gan, Z. and Xie, Y. (2017) Mechanism of non-appearance of hiatus in Tibetan Plateau. *Scientific Reports*, 7, 4421.

Pearson, R.G., Phillips, S.J., Loranty, M.M., Beck, P.S.A., Damoulas, T., Knight, S.J., Goetz, S.J. (2013) Shifts in Arctic vegetation and associated feedbacks under climate change. *Nature Climate Change*, 3, 673–677.

Pepin, N.C., Bradley, R.S., Diaz, H.F., Diaz, H.F., Baraer, M., Caceres, E.B., Forsythe, N., Fowler, H., Greenwood, G., Hashmi, M.Z., Liu, X., Miller, J.R., Ning, L., Ohmura, A., Palazzi, E., Rangwala, I., Schöner, W., Severskiy, I., Shahgedanova, M., Wang, M., Williamson, S.N. & Yang, D. (2015) Elevation-dependent warming in mountain regions of the world. *Nature Climate Change*, 5, 424–430. https://doi.org/10.1038/nclimate2563.

Pickart, R.S. and Spall, M.A. (2007) Impact of Labrador Sea convection on the North Atlantic Meridional overturning circulation. *Journal of Physical Oceanography*, 37, 2207–2227.

Qiu, J. (2008) China: the third pole. *Nature*, 454, 393–396.

Rangwala, I., Sinsky, E. and Miller, J.R. (2013) Amplified warming projections for high altitude regions of the Northern Hemisphere mid-latitudes from CMIP5 models. *Environmental Research Letters*, 8, 024040. https://doi.org/10.1088/1748-9326/8/2/024040.

Shen, M., Piao, S., Jeong, S.J., Zhou, L., Zeng, Z., Ciais, P., Chen, D., Huang, M., Jin, C.S., Li, L.Z.X., Li, Y., Myneni, R.B., Yang, K., Zhang, G., Zhang, Y. and Yao, T. (2015) Evaporative cooling over the Tibetan Plateau induced by vegetation growth. *Proceedings of the National Academy of Sciences of the United States of America*, 112, 9299–9304.

Shi, C., Sun, C., Wu, G., Wu, X., Chen, D., Masson-Delmotte, V., Li, J., Xue, J., Li, Z., Ji, D., Zhang, J., Fan, Z., Shen, M., Shu, L. and Ciais, P. (2019) Summer temperature over the Tibetan Plateau modulated by Atlantic multidecadal variability. *Journal of Climate*, 32, 4055–4067.

Shi, S., Li, J., Shi, J., Zhao, Y. and Huang, G. (2017) Three centuries of winter temperature change on the southeastern Tibetan Plateau and its relationship with the Atlantic multidecadal oscillation. *Climate Dynamics*, 49, 1305–1319.

Sui, Y., Jiang, D. and Tian, Z. (2013) Latest update of the climatology and changes in the seasonal distribution of precipitation over China. *Theoretical and Applied Climatology*, 113, 599–610.

Takaya, K. and Nakamura, H. (2001) A formulation of a phase-independent wave-activity flux for stationary and migratory quasigeostrophic eddies on a zonally varying basic flow. *Journal of the Atmospheric Sciences*, 58, 608–627.

Trenberth, K.E. (2011) Changes in precipitation with climate change. *Climate Research*, 47, 123–138.

Wang, B., Bao, Q., Hoskins, B., Wu, G. and Liu, Y. (2008) Tibetan Plateau warming and precipitation changes in East Asia. *Geophysical Research Letters*, 35, L14702.

Wang, J., Yang, B., Ljungqvist, F.C. and Zhao, Y. (2013a) The relationship between the Atlantic multidecadal oscillation and temperature variability in China during the last millennium. *Journal of Quaternary Science*, 28, 653–658.

Wang, J., Yang, B., Qin, C., Kang, S., He, M. & Wang, Z. (2013b) Tree-ring inferred annual mean temperature variations on the southeastern Tibetan Plateau during the last millennium and their relationships with the Atlantic multidecadal oscillation. *Climate Dynamics*, 43, 627–640.

Wang, X., Yang, M., Liang, X., Pang, G., Wan, G., Chen, X. and Luo, X. (2014) The dramatic climate warming in the Qaidam Basin, northeastern Tibetan Plateau, during 1961–2010. *International Journal of Climatology*, 34, 1524–1537.

Watanabe, M. and Kimoto, M. (2000) Atmosphere Ocean thermal coupling in the North Atlantic: a positive feedback. *The Quarterly Journal of the Royal Meteorological Society*, 126, 3343–3369.

Watanabe, M., Kimoto, M. and Nitta, T. (1999) A comparison of decadal climate oscillations in the North Atlantic detected in observations and a coupled GCM. *Journal of Climate*, 12, 2920–2940.

Weare, B.C. and Nasstrom, J.S. (1982) Examples of extended empirical orthogonal function analyses. *Monthly Weather Review*, 110, 481–485.

Weare, B.C. and Newell, R.E. (1977) Empirical orthogonal analysis of Atlantic Ocean surface temperatures. *The Quarterly Journal of the Royal Meteorological Society*, 103, 467–478.

Wu, G., Liu, Y., He, B., Bao, Q., Duan, A. and Jin, F.F. (2012) Thermal controls on the Asian summer monsoon. *Scientific Reports*, 2, 4.

Wu, Y., Yang, S., Hu, X. and Wei, W. (2020) Process-based attribution of long-term surface warming over the Tibetan Plateau. *International Journal of Climatology*. https://doi.org/10.1002/joc.6589.

Xu, X., Lu, C., Shi, X., Gao, S., Xu, A., Lu, X., Shi, C. and Gao, X. (2008) World water tower: an atmospheric perspective. *Geophysical Research Letters*, 35, L20815.

Xu, X., Zhao, T., Lu, C., Guo, Y., Chen, B., Liu, R., Li, Y. and Shi, X. (2014) An important mechanism sustaining the atmospheric "water tower" over the Tibetan Plateau. *Atmospheric Chemistry and Physics*, 14, 11287–11295.

Yan, L., Liu, Z., Chen, G., Kutzbach, J.E. and Liu, X. (2016) Mechanisms of elevation-dependent warming over the Tibetan Plateau in quadrupled CO2 experiments. *Climatic Change*, 135, 509–519. https://doi.org/10.1007/s10584-016-1599-z.

Yao, T., Thompson, L., Yang, W., Yu, W., Gao, Y., Guo, X., Yang, X., Duan, K., Zhao, H. and Xu, B. (2012) Different glacier status with atmospheric circulations in Tibetan Plateau and surroundings. *Nature Climate Change*, 2, 663–667.

You, Q., Fraedrich, K., Ren, G., Ye, B., Meng, X. and Kang, S. (2012) Inconsistencies of precipitation in the eastern and central Tibetan Plateau between surface adjusted data and reanalysis. *Theoretical and Applied Climatology*, 109, 485–496.

You, Q., Min, J. and Kang, S. (2016) Rapid warming in the Tibetan Plateau from observations and CMIP5 models in recent decades. *International Journal of Climatology*, 36, 2660–2670.

You, Q., Min, J., Zhang, W., Pepin, N. and Kang, S. (2015) Comparison of multiple datasets with gridded precipitation observations over the Tibetan Plateau. *Climate Dynamics*, 45, 791–806.

Zhang, R. (2010) Latitudinal dependence of Atlantic meridional overturning circulation (AMOC) variations. *Geophysical Research Letters*, 37, L16703.

Zhang, R., Sutton, R., Danabasoglu, G., Kwon, Y.-O., Marsh, R., Yeager, S.G., Amrhein, D.E. and Little, C.M. (2019) A review of the role of the Atlantic Meridional overturning circulation in Atlantic multidecadal variability and associated climate impacts. *Reviews of Geophysics*, 57, 316–375 https://doi.org/10.1029/2019RG000644.

Zhang, Y., Wang, D., Zhai, P., Gu, G. and He, J. (2013) Spatial distributions and seasonal variations of tropospheric water vapor content over the Tibetan Plateau. *Journal of Climate*, 26, 5637–5654.

Zhao, Y. and Zhou, T. (2019) Asian water tower evinced in total column water vapor: a comparison among multiple satellite and reanalysis data sets. *Climate Dynamics*, 54, 231–245.

Zhou, X., Zhao, P., Chen, J., Chen, L. and Li, W. (2009) Impacts of thermodynamic processes over the Tibetan Plateau on the northern hemispheric climate. *Science in China. Series D, Earth Sciences*, 52, 1679–1693.

How to cite this article: Gao K, Duan A, Chen D. Interdecadal summer warming of the Tibetan Plateau potentially regulated by a sea surface temperature anomaly in the Labrador Sea. *Int J Climatol*. 2020;1–11. https://doi.org/10.1002/joc.6871